

Photonic Curing of Low-Cost Aqueous Silver Flake Inks for Printed Conductors with Increased Yield

Harry M. Cronin,^{†,§} Zlatka Stoeva,[†] Martin Brown,[‡] Maxim Shkunov,[§] and S. Ravi P. Silva^{*,§,✉}

[†]DZP Technologies Ltd., Future Business Centre, Kings Hedges Road, Cambridge CB4 2HY, U.K.

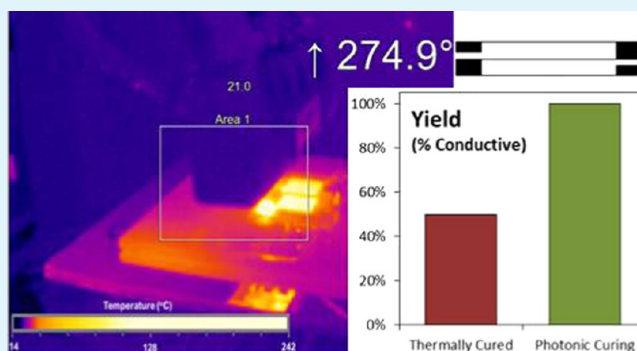
[‡]Heraeus Noblelight Ltd., Cambridge Science Park, Milton Road, Cambridge CB4 0GQ, U.K.

[§]Advanced Technology Institute, University of Surrey, Guildford, Surrey GU2 7XH, U.K.

Supporting Information

ABSTRACT: Printing of highly conductive tracks at low cost is of primary importance for the emerging field of flexible, plastic, and large-area electronics. Commonly, this is achieved by printing of metallic conductive inks, often based on Ag or Cu nanoparticles dispersed in organic solvents. The solvents, which must be safely removed, have particular storage and handling requirements, thus increasing the process costs. By using water-based inks containing micron-sized silver flakes, both material and process costs can be reduced, making these inks attractive for industrial applications. However, the sintering of flake inks requires higher temperatures than nano-sized inks owing to the particles' smaller surface area-to-volume ratio, meaning that when cured thermally the conductivity of many flake inks is lower than nanoparticle alternatives. This problem can be addressed by the application of visible light photonic curing; however, the substrate must be protected and so process parameters must be defined for each material/substrate combination. Here, we report results of a large-scale trial of photonic curing of aqueous flake silver inks on poly(ethylene terephthalate) substrates in an industrial setting. The resistivity of printed patterns after an optimized photocuring regime matched those reported for typical nanoparticle inks; on the order of $100 \mu\Omega \text{ cm}$ depending on substrate and geometry. Scanning electron microscopy revealed evidence for structural changes within the printed films consistent with localized melting and necking between adjacent particles, leading to an improved percolation network. Furthermore, in the large-scale industrial trial employing screen-printed silver lines, the manufacturing yield of conductive lines was increased from 44% untreated to 80% after photocuring and reached 100% when photocuring was combined with thermal curing. We believe this to be the first reported observation of an increase in the yield of printed electronic structures following photocuring. We propose a crack-healing mechanism to explain these increases in yield and conductivity. We further report on the effects of the photonic curing on the mechanical bending stability of the printed conductors and discuss their suitability for wearable applications.

KEYWORDS: photonic curing, intense pulsed light, aqueous inks, printed electronics, silver conductive inks



1. INTRODUCTION

The rapidly growing field of flexible plastic electronics promises to enable high volume production of electronic devices via large-scale, roll-to-roll processes. Such devices have much lower production costs than traditional methods of electronics manufacture due to their non-vacuum and low-temperature-based processes and can be made on flexible plastic or paper substrates along with other novel form factors.^{1,2} Lately, silver inks are becoming more important as the conductive material of choice for printed electronics. Current applications of silver inks include printed solar cells, where silver layers may either be used in a grid structure as transmitting electrodes or in a bulk layer structure as back contacts.^{3–5} Printed silver structures have also been successfully demonstrated in organic light-emitting diodes,⁴ radio frequency identification antennae,⁶ and electrodes for touch screens.⁷ In all of these applications,

despite how good the bulk conductivity of the pure silver material may be, the conductivity of the printed layers will vary widely because the silver needs to be applied and patterned via a suitable ink and printing process. Therefore, the morphology of the printed patterns, and crucially the percolation networks formed between the nano- or micron-scale particles of the conductive material, will drive the conductivity values achieved. Homogeneity of the printed layer and adhesion to flexible substrates are further key performance parameters.⁸

Current commercially available silver inks for applications on flexible substrates are often based on silver nanoparticles, which require expensive and time-consuming synthesis techniques. A

Received: March 13, 2018

Accepted: June 4, 2018

Published: June 4, 2018

lower-cost alternative is copper nanoparticle or flake inks, but these are prone to oxidation.⁹ In many cases, nanoparticle inks use volatile organic solvents, which may require specific solvent handling measures to be implemented in the production, storage, and transportation, thus further driving up the overall system costs.¹⁰ A water-based, low-cost ink is therefore desirable, and one approach is to move to micron-sized silver flakes, which are generally significantly cheaper than silver nanoparticles due to their higher-yielding synthesis methods.¹¹ Conductive flake inks are commonly used in applications that can tolerate high temperatures needed to sinter the flakes (usually >800 °C), including photovoltaic applications^{12,13} and ceramic tapes.¹⁴ As a further advantage of flake inks, the high aspect ratio of the flakes could have advantages in terms of the stretchability and flexibility of printed conductive structures. This is becoming a key consideration in ink materials research due to the trend toward wearable electronic devices.

Many functional inks require curing and/or sintering to become conductive. Here, the term curing is used to mean the removal of residual solvents and cross-linking of binders, whereas sintering is used to mean the densification of particles driven by surface free energy minimization, leading to increased interparticle contact. Owing to the melting point suppression of nanoparticles caused by their very high surface area-to-volume ratios,¹⁵ full sintering can often be achieved in these systems within a temperature range tolerable to the substrate.¹⁶ Flake inks, however, have the same melting point as the bulk material, so full sintering is not usually possible within such a temperature range. Therefore, the conductivity that can be achieved with such inks is often lower than that of nanoparticle-based inks. To improve conductivity with flake inks, we have applied broadband intense pulsed light photocuring to screen printed conductive traces.

Broadband photonic curing, consisting of exposing the samples to short pulses of high-intensity light, is a technique that has been known for a number of years and commonly applied to the sintering of nanoparticle-based inks based on both copper and silver.^{9,16–22} Although a range of curing and sintering methods are available, including pure thermal curing, or a range of Ohmic, optical, and plasma- or microwave-assisted technologies,^{16,23–26} the advantages of photonic curing include its high speed, wide coverage area, and ability to heat the printed layer to a much higher temperature than the substrate.²⁷ Photonic curing is commonly used where there is a need to keep flexible plastic substrates below their glass transition temperature.¹⁶ However, the maximum temperature that can be tolerated within the printed structure is also limited by the need to avoid potentially damaging decomposition of the binders within the printed layer, which would lead to mechanical failure. Therefore, photonic curing settings must be defined for each new material/substrate combination.

Probably due to these factors, combined with their higher temperature curing requirements, relatively little work has been reported on photocuring of flake inks. Tam et al.²⁸ applied intense pulsed light sintering to a Cu ink with mixed nanoparticles and flakes; however, the main sintering effect was attributed to the nanoparticles. Park et al. applied IR curing to flake silver inks, showing a reduction in sheet resistance, but this technique has a lower power density and a longer treatment time than visible-light photocuring.²⁹ Cui et al. reported photonic curing of electrically conductive adhesives containing silver flakes.³⁰ Although in this work the authors' aim was to cross-link the polymers to form an adhesive bond,

they did report the observation of a sintering effect on the silver flakes; however, it required the use of very high power densities, and the authors noted that the adhesion within the deposited layer was severely reduced. Therefore, if a photonic processing technique can be demonstrated that improves the conductivity of Ag flake inks while retaining good adhesion in the printed layers as well as protecting the poly(ethylene terephthalate) (PET) substrates, this would be advantageous for industrial applications.

Here, we demonstrate that despite their higher melting point compared with nanoparticles, visible-light photonic curing can be used to cause interparticle necking of flake silver inks of average flake sizes 1–3 μm , and thereby improve the existing percolation network for charge conduction, without destroying the adhesion in the printed layer or damaging the substrate. In addition to the removal of solvent and some binder, such necking between adjacent flakes greatly increases the conductivity by increasing the contact area between adjacent flakes and introducing additional percolation pathways.

Furthermore, we present for the first time results of a large-scale trial of such a technique carried out in an industrial setting. This trial revealed an increase in manufacturing yield after the photonic curing. This observation is explained by a crack-healing process in the samples as a result of photonic curing, in which the observed interparticle necking is able to bridge cracks in the samples. Because very fine cracks are a common failure mode in the manufacture of printed lines, this allows many nonconductive structures to be repaired in-line. In a typical screen-printed interconnect application, this crack healing led to an increased yield of conductive lines from 44% untreated to 80% using photonic curing alone, and 100% when photonic curing was combined with thermal curing. Increased manufacturing yield is a vital consideration, along with choice of ink formulation and solvent, to reduce the overall process costs within industrial settings. Note that here we use the term manufacturing yield to refer to the percentage of printed lines that are conductive.

2. EXPERIMENTAL PROCEDURE

Poly(ethylene terephthalate) (PET) substrates were cleaned using an isopropyl alcohol wash followed by contact cleaning with an adhesive roller system (Teknek). The samples were screen printed using a 400 mesh stainless steel screen from aqueous Ag inks with 1–3 μm Ag flake size, 60 wt % Ag (DZP Technologies, Cambridge, U.K.). The samples were separated into four groups: control, photonic treatment only, thermal treatment only, and thermal plus photonic treatment. The control group was held with no further treatment. The samples requiring thermal curing were baked under ambient atmospheric conditions in an oven at 120 °C for 1.5 h. Note that the curing temperature of 120 °C was set by the maximum tolerable by the PET substrate, which begins to deform above this temperature.

Photonic treatment was carried out using a Xenon flash lamp system (Heraeus Noblelight Ltd., Cambridge, U.K.). A typical regime consisted of 3 consecutive pulses of 3 ms duration at a frequency of 100 Hz, using a 400 V lamp input voltage with a 30 mm working distance under ambient atmospheric conditions. These conditions were measured to correspond to an energy input of approximately 1.0 J/cm² to the samples. A Ce-doped glass envelope was used on the lamp to reduce UV exposure, which might be damaging to both polymeric binders in the ink and the substrate.

The samples were characterized electrically using a Keithley 4200 SCS source meter. Sheet resistance was measured using a custom-built four-point probe head with spring-loaded, copper-coated probe tips spaced linearly with a 3 mm tip separation. The resistivity of the fine lines was measured according to the standard ASTM F1896-10 using

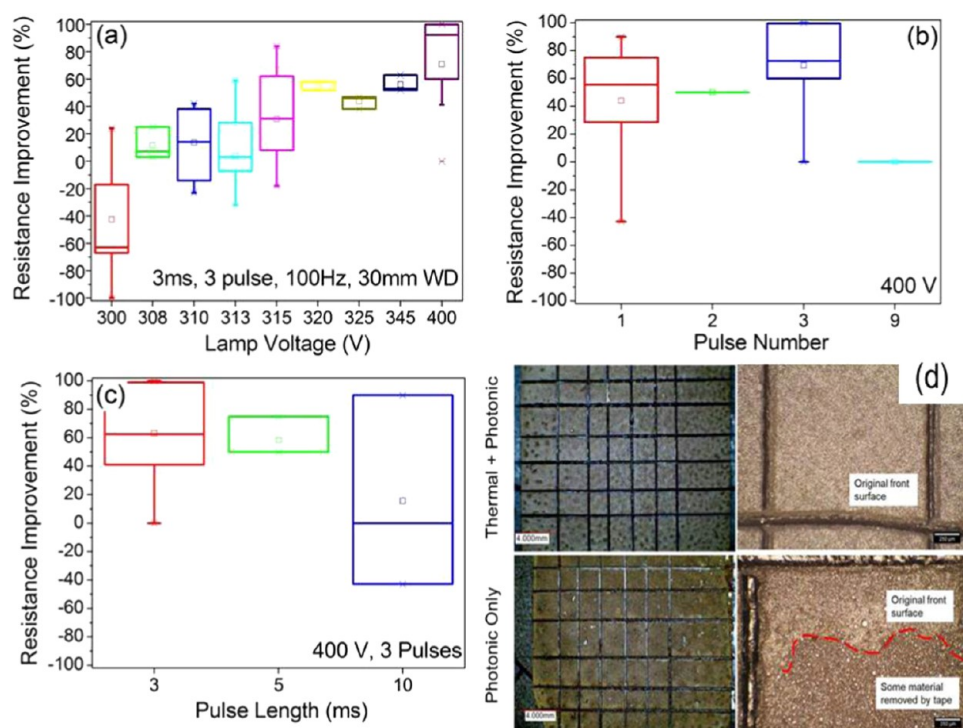


Figure 1. Optimization of the lamp settings for the silver flake inks. Lamp voltage (a) was first optimized and a setting of 400 V was used for further trials. Pulse number (b) and length (c) were found to have less of an effect on the resistance of the samples. Optical micrographs (d) of the samples after cross-cut tape peel testing, with areas of material removal demarcated with red dashed line.

specially-adapted probe tips to avoid damaging the samples. The cross-sectional area of the printed lines was measured at several points along each sample using an optical microscope. Scanning electron microscopy (SEM) was carried out using an FEI Quanta ESEM in secondary electron mode at an accelerating voltage of 10 kV. Adhesion testing was carried out by cross-cut tape peel testing.

Bend testing was carried out using a home-built testing rig, which bends the samples around a radius of 20 mm. Bending occurred at 2.5 Hz, and the samples were returned to the flat state between each bend. The electrodes were attached by conductive adhesive to the sample terminals and a current of between 1 and 100 mA applied by an external power source. The resulting voltage drop along each trace as a function of time was monitored by a PicoLog 1000 data logger (Pico Technologies) and used to calculate the resistance of each trace as a function of the number of bends.

3. RESULTS AND DISCUSSION

3.1. Optimization of Lamp Settings. The lamp settings were first optimized by using $20 \times 20 \text{ mm}^2$ printed squares (termed “bulk” samples). Two factors were used for the optimization: the conductivity improvement achieved and the presence of any damage to the sample. In some cases, sample damage is immediately obvious (where significant ablation or blow-off occurs), whereas in other cases, it was revealed by subsequent adhesion testing. The lamp parameters varied were voltage, pulse number, and pulse length, whereas working distance was fixed at 30 mm and frequency at 100 Hz (with the exception of 10 ms pulses, which were carried out at 50 Hz to allow some off-time). The resistance of printed squares was measured before and after exposure, and the resistance improvement ratio (defined as the difference in resistance before and after the treatment, divided by the initial resistance) was used to quantify the effect of the treatment. Summary results are shown in Figure 1.

As discussed by Niittynen et al.,²² when working distance is fixed, lamp voltage is the main factor affecting the optical power input to the samples. This is reflected in the results shown in Figure 1, where we find that by far the largest factor determining the improvement in resistance is the lamp voltage (Figure 1a), with voltages less than 400 V tending to have less positive impact on the resistance. The maximum voltage available in the experiment was 400 V, and this was found to be necessary to cause a reduction in the resistance in the majority of samples. Unexpectedly, at voltages of 300 V, there were significant number of samples showing negative values for the “resistance improvement” measurement (implying resistance has increased). It is likely that this resistance increase arises due to damage to the samples caused by incomplete curing through the depth of the sample, in which the lamp energy is not sufficient to cause any beneficial curing effect, but is sufficient to cause blow-off or otherwise damage the samples. When the lamp voltage is increased from 300 to 308 V, there is a dramatic change in this behavior, likely indicating the onset of a beneficial sintering effect that compensates for any sample damage seen. This is maintained for subsequent higher lamp voltages up to the maximum of 400 V. Therefore, 300 V appears to be the threshold voltage beyond which improved conduction can result for these conditions of 3 ms, 3 pulses, and 100 Hz lamp.

Having fixed the voltage at 400 V, the number of consecutive pulses (at 100 Hz) was varied. Figure 1b demonstrates that this parameter has a less dramatic impact on performance than lamp voltage, with 3 pulses here found to be optimum. Finally, with voltage set at 400 V and pulse number set at 3, the pulse length was varied. Although pulse length would be expected to determine the overall energy input, this relationship is nonlinear due to droop of the capacitors in the power supply over time. However, as pulse length was increased from 3 to 10

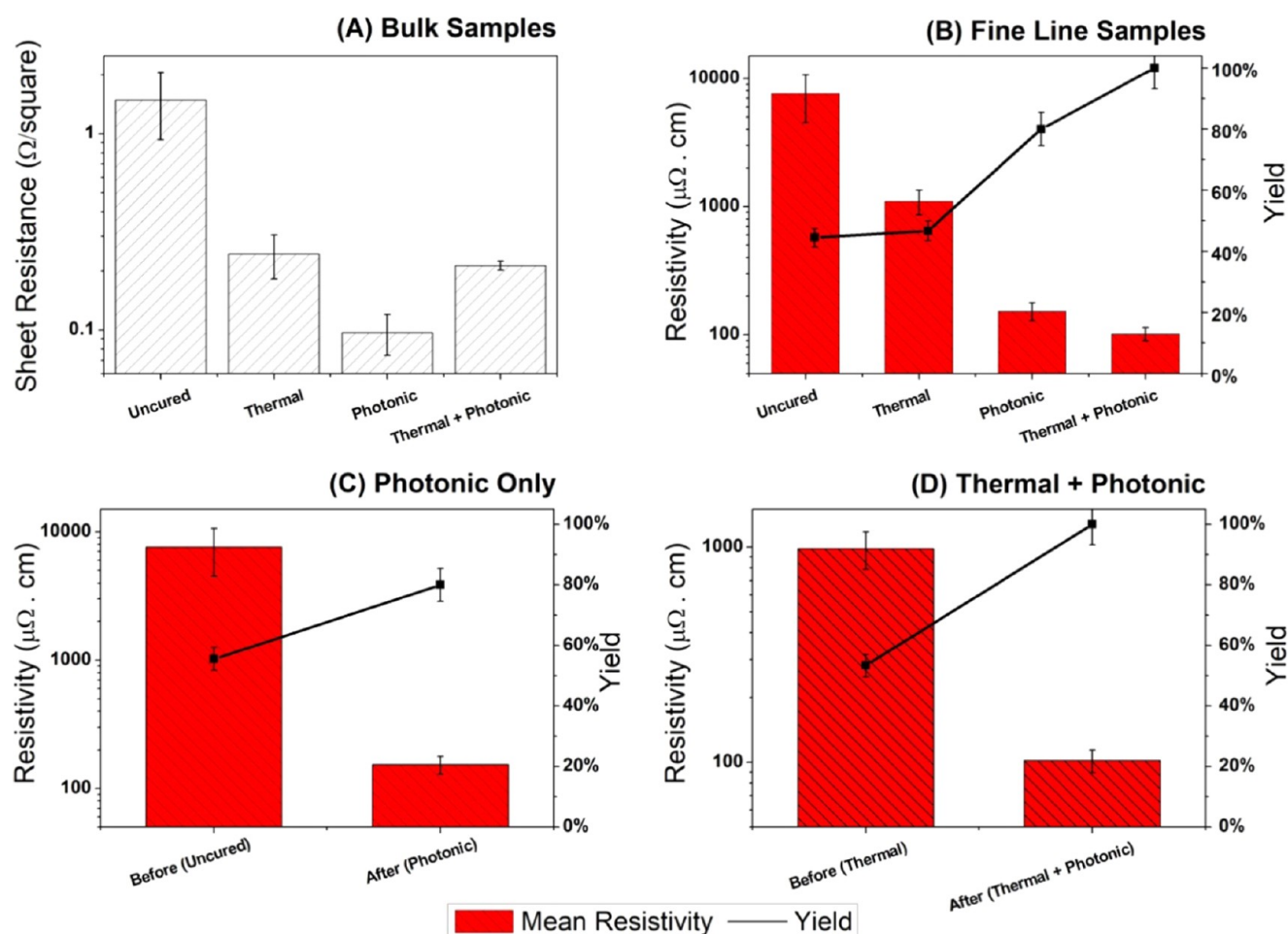


Figure 2. Sheet resistance of bulk samples (A). Resistivity and yield of the fine line samples, cured with (B) all four regimes, (C) photonic curing only (before and after photocuring), and (D) thermal plus photonic curing (also before and after). Error bars on resistivity show standard error of the mean and on yield show standard deviation between several groups of samples.

ms, the number of samples that were noticeably damaged by the photonic treatment increased, which is reflected in the trend toward more negative values of the resistance improvement at longer time scales. Based on these measurements, lamp settings of 400 V and 3 pulses of 3 ms length at 100 Hz were used for the remainder of the study.

Finally, it was found that in some cases it was possible to greatly improve the resistance of the samples by using “extreme” lamp settings (for example, very long pulses), but that this had a detrimental impact on the adhesion between the sample and the substrate due to excessive removal of the polymer binder. To explore this effect, bulk samples that had been photocured using the optimized settings were further characterized by tape-peel adhesion testing according to ASTM D3359-09, using a scotch tape. This standard defines six classes depending on the amount of material removed by the tape, from class 5B (no removal) to class 0B (major removal). Whereas all the samples in the control, thermal, and thermal-photonic samples showed good adhesion, with the tape removing little or no material (<5% material removed, class 4B), approximately 50% of the samples in the photonic-only group showed poor adhesion, with a large amount of material removed by the tape (class 1B, 35–65% material removed). Optical microscopy (Figure 1d) showed that the failure in these samples was not an adhesive or interfacial failure between the printed layer and the substrate, but rather a cohesive failure

within the layer. This cohesive failure likely points to the existence of a two-layer structure that has developed within the silver layer as a result of the photonic treatment being applied directly to the uncured samples, which have not fully dried because the samples that had been given >24 h drying time between printing and photocuring did not show this effect. This effect does not affect the conclusions drawn here, but would need to be accounted for in future applications, in which it is highly likely that a step curing regime can be adopted to ensure there is no cohesive failure within the printed layer, while still delivering the desired conductivity improvement.

3.2. Photonic Curing of Bulk Samples. Using optimized settings, a batch of 18 bulk samples were treated in one of four different ways: untreated (control), thermal cure only, photonic only, or thermal plus photonic curing. The sheet resistance of the samples in the four groups was then measured. The results of the electrical characterization are outlined in Figure 2A. Note that because we measure the sheet resistance and resistivity throughout this work, the desirable outcome is a reduction in these values (showing an increase in the conductivity of the sample). The uncured samples showed a relatively high sheet resistance with a high standard deviation, of around $1.5 \pm 0.6 \Omega/\text{sq}$, at a thickness of $25.4 \mu\text{m}$ (1 mil). This is as would be expected from an ink that has simply been deposited and dried at room temperature with no further treatment. Both thermal and photonic curing regimes led to a large reduction in sheet

resistance and standard deviation. Average sheet resistance after thermal treatment was $0.24 \pm 0.06 \text{ } \Omega/\text{sq}$, photonic treatment led to an average sheet resistance of $0.1 \pm 0.02 \text{ } \Omega/\text{sq}$, and thermal plus photonic treatment to an average sheet resistance of $0.2 \pm 0.01 \text{ } \Omega/\text{sq}$. The difference between the photonic-only and thermal-plus-photonic batches is likely to be due to the increased reflectivity of the ink after thermal curing. The sheet resistance of the most conductive individual sample achieved with photonic curing was $0.05 \text{ } \Omega/\text{sq}$, which compares favorably with the reports for nanoparticle inks, which range from 0.05 to $0.35 \text{ } \Omega/\text{sq}$ at $25 \text{ } \mu\text{m}$ thickness, depending on the substrate and curing used.³¹ The yield of this type of sample was 100% in all the cases.

3.3. Photonic Curing of Fine Lines. Using the optimized regime arrived at above, we then proceeded to cure screen-printed fine line samples, consisting of a batch of 93 lines with a mean width of $90 \text{ } \mu\text{m}$, mean thickness $13 \text{ } \mu\text{m}$, and length (defined by the placement of measurement pads) of 30 mm . The electrical characterization of fine line samples is shown by the bar chart in Figure 2B, where the height of the bars shows the mean resistivity and the error bars show standard error. Uncured samples showed a mean resistivity of $7590 \pm 3080 \text{ } \mu\Omega \text{ cm}$; thermal curing improved this to $1100 \pm 230 \text{ } \mu\Omega \text{ cm}$; photonic curing alone showed a significant further improvement in resistivity to $153 \pm 25 \text{ } \mu\Omega \text{ cm}$; and the best results were achieved when combining thermal and photonic curing, which led to a resistivity of $100 \pm 12 \text{ } \mu\Omega \text{ cm}$, whereas the most conductive individual sample had a resistivity of $60 \pm 6 \text{ } \mu\Omega \text{ cm}$. Therefore, compared with uncured samples, thermally cured samples showed on an average $6.9\times$ lower resistivity, whereas samples that were photonicly cured showed resistivities on an average $50\times$ lower and thermal plus photonicly cured samples showed on an average $75\times$ lower resistivities, which represent a $10\times$ resistivity improvement, along with reduction in standard deviation, over thermal curing alone. More detailed comparisons between uncured and photonicly cured and between thermally cured only and thermal followed by photonic curing are shown in Figure 2C,D, respectively.

The thermal curing regime used in this work consisted of 1.5 h at $120 \text{ } ^\circ\text{C}$. This maximum temperature is limited by the PET substrate, which begins to deform at around $130 \text{ } ^\circ\text{C}$. A measurement of the resistance of printed tracks as a function of time (Supporting Information, Figure S1) showed that after 1.5 h, there is no further improvement in resistance. Therefore, the samples in the thermal group represent the optimal conductivity achievable by thermal means with this particular substrate. As a comparison, the same ink was printed on the glass slide and cured at $220 \text{ } ^\circ\text{C}$ (above this temperature, browning of the binder was observed on some samples). These samples had a mean resistivity of $100 \pm 25 \text{ } \mu\Omega \text{ cm}$; comparable to that of photocured samples. However, owing to different substrate (rigid vs flexible), these values are not directly comparable.

When comparing the results of this thermal curing with photonic curing, from the present results, it appears that although both significantly reduce the resistance compared to uncured samples, the lowest achievable resistance by thermal curing is significantly higher than that achievable by photonic curing. This is likely due to the localized higher temperatures, which can be achieved in the printed pattern by photonic curing.

A further difference observed here between thermal curing and photonic curing is the change in yield (percentage of lines

that showed end-to-end conductivity). As shown in Figure 2B, there was no significant change in the yield after thermal curing; in both cases, approximately 45% of the samples were conductive end-to-end. The small difference in yield shown in Figure 2B (44% uncured vs 47% thermally cured) is within the error of the measurement. When comparing the thermal group before and after thermal curing, the yield was 47% in both cases. As such, thermal curing had no effect on the yield. In contrast, both sets of samples that were photonicly cured showed dramatic improvements in yields from 56 to 80% (photonic only) and from 53 to 100% (thermal plus photonic). The difference between 80% yield seen after photonic curing and 100% seen after thermal-plus-photonic curing may be due to the former process taking completely uncured samples as the starting point, meaning that significantly higher levels of unremoved water are present, leading to increased risk of sample blow-off and ablation. From these drastic yield improvements, and considering that these are the same samples measured before and after treatment, we can conclude that some lines that were nonconductive before photonic curing (resistance $>20 \text{ M}\Omega$) became highly conductive after the treatment. This observation of an increase in yield, taken together with the large additional increase in conductivity seen with photonic-based treatments compared with purely thermal curing, implies that physical changes may be occurring in the samples over and above the removal of solvent and cross-linking of binder expected with thermal curing. To investigate this hypothesis, we first calculated the expected temperature rise in the samples as a function of depth and time.

3.4. Calculation and Measurement of the Expected Temperature Rise. The expected temperature rise in the printed layers as a function of thickness and time can be calculated using an analytical solution to the heat transfer partial differential equation as a function of depth z and time t . For uniform light input, this was solved by Carslaw and Jaeger,³² and a simplified form of the solution given by Çengel³³ is

$$\Delta T(z, t) = \frac{2[I(1 - R)]}{k} \sqrt{\alpha t} \times \text{ierfc} \left[\frac{z}{2\sqrt{\alpha t}} \right] \quad (1)$$

where α is the thermal diffusivity of the printed layer, I is the light intensity, R is the surface reflectivity, k is the thermal conductivity of the printed layer, and ierfc is the integral of the complementary error function.

To solve eq 1, several material parameters of the printed but uncured layers must be calculated. We estimate the thermal conductivity k on the basis of the Maxwell equation,³⁴ an approximate aspect ratio of the flakes of $1/3$, and using the known volume fractions of silver flakes and binder, which yields a value of around $0.07 \text{ W}/(\text{m K})$. Similarly, the density of the printed layers was calculated from the ratios of the ink constituents based on a rule of mixtures approach and found to be $8200 \text{ kg}/\text{m}^3$. The specific heat capacity was calculated according to Kopp's law from the individual heat capacities and found to be $880 \text{ J}/(\text{kg K})$. These values yield a value of the thermal diffusivity $\alpha = 9.6 \times 10^{-9} \text{ m}^2/\text{s}$.

It should be noted that the low estimated value of the thermal conductivity k of the printed but uncured layers is in agreement with the low electrical conductivity of such layers measured in the present work. This would be expected from the consideration of Wiedemann–Franz law, which states that the ratio of thermal to electrical conductivity in metals at

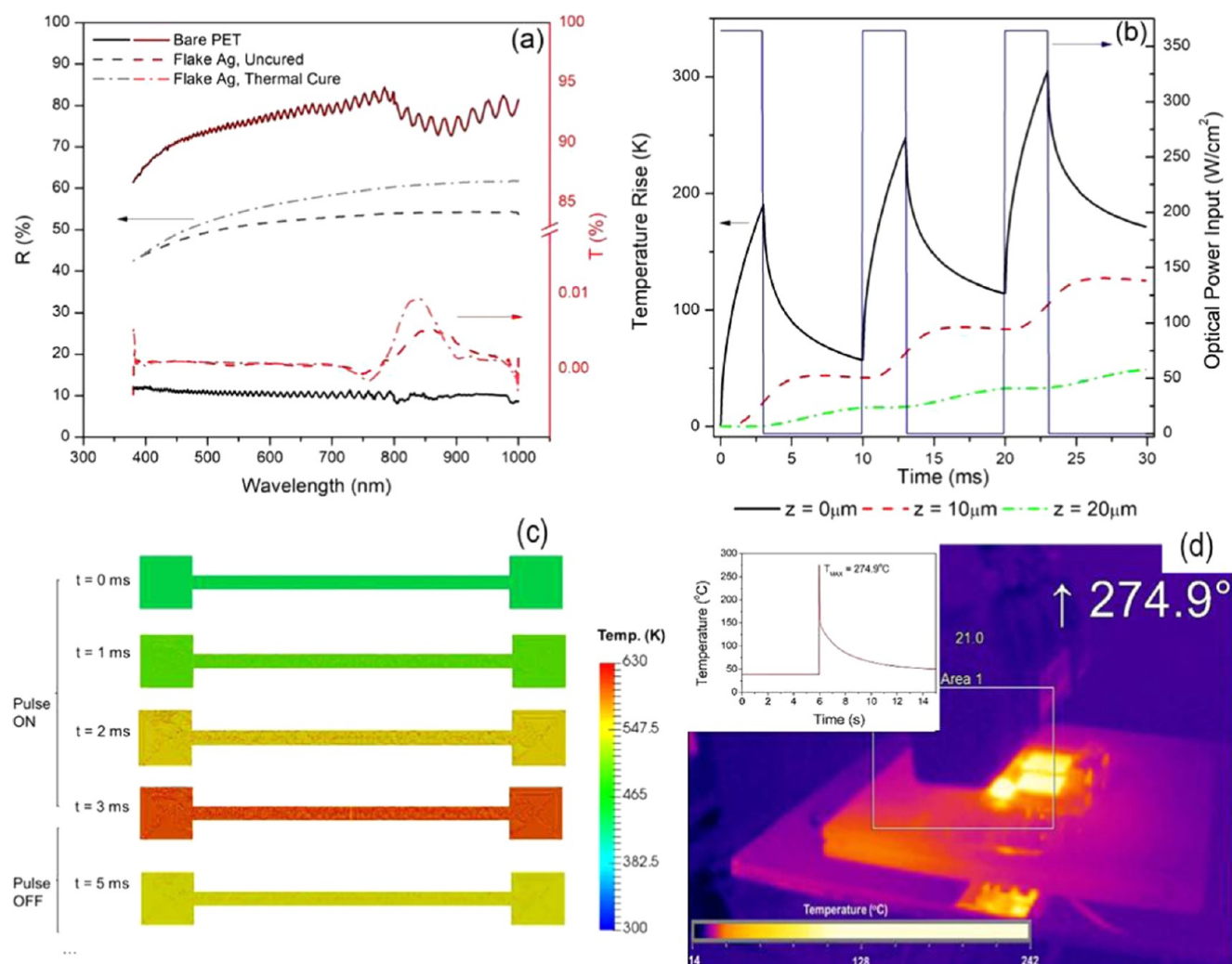


Figure 3. Optical transmittance and reflectance (a) of silver ink samples by UV–vis spectrometry. Temperature evolution as a function of depth (b) after photocuring for three 3 ms pulses at 100 Hz. Results of a finite-element model (c) showing the temperature on the front surface of an Ag line for the third 3 ms pulse in a group of 3 pulses. Radiometric temperature measurement (d) of the sample area.

constant temperature is a constant.^{35,36} Because the electrical conductivity was measured as being low in uncured samples, and the only electrically conductive species present is silver metal, it would be expected that the thermal conductivity would also be low; this effectively represents a situation where a large fraction of the silver flakes are not part of an end-to-end percolation network.

In this model, the printed layer is approximated as being semi-infinite, and heat conduction within the layer is assumed to dominate over convection to the outside air. The validity of the semi-infinite approximation can be checked by calculating the critical length L_c in which heat is expected to diffuse in time t , using $L_c = (4\alpha t)^{1/2}$, which for a pulse length of 3 ms gives a distance of $10.7 \mu m$,³⁷ or approximately half the film thickness in this model, which justifies the use of the approximation. Therefore, we can have confidence in the results of this model as long as the samples' thickness is $>10.7 \mu m$ because finite sample thickness or substrate effects do not affect heat diffusion (within 3 ms) above this limit. This was the case in our experiment. Further, the sample width will only affect the temperature rise if the sample is large enough so that part of it falls outside the uniform area of the beam. This was not the case in our experiment, where the energy profile of the beam is

highly uniform over the frontal area of the samples. This represents an advantage of broadband photonic curing over laser-based methods because large areas are treated simultaneously. Finally, the dominance of heat conduction within the samples over convection or radiation from the surface is a valid assumption if the temperature remains below approximately $1000^{\circ}C$,³⁸ which is a valid consideration for our experiment.

The optical power density input I was calculated by integration of the output spectrum of the lamp (supplied by the manufacturer) over the wavelength range of interest. This output spectrum was measured for a 3 ms pulse at 400 V. To estimate a value for the reflectivity R of the ink surface, UV–vis spectrometry was employed. These results are shown in Figure 3a. The reflectivity of the silver ink is relatively flat in the wavelength range of interest, with a slight reduction at short wavelengths. This reflects the fact that the reflectivity of silver inks is dominated by scattering from the silver particles, rather than approximating the value of pure silver.³⁹

Solving eq 1 for t and varying z for a printed but uncured silver flake/binder layer gives a temperature profile, which is shown in Figure 3b. The same calculation for cured layers (Supporting Information, Figure S2) showed similar behavior, but with both maximum surface temperature and back surface

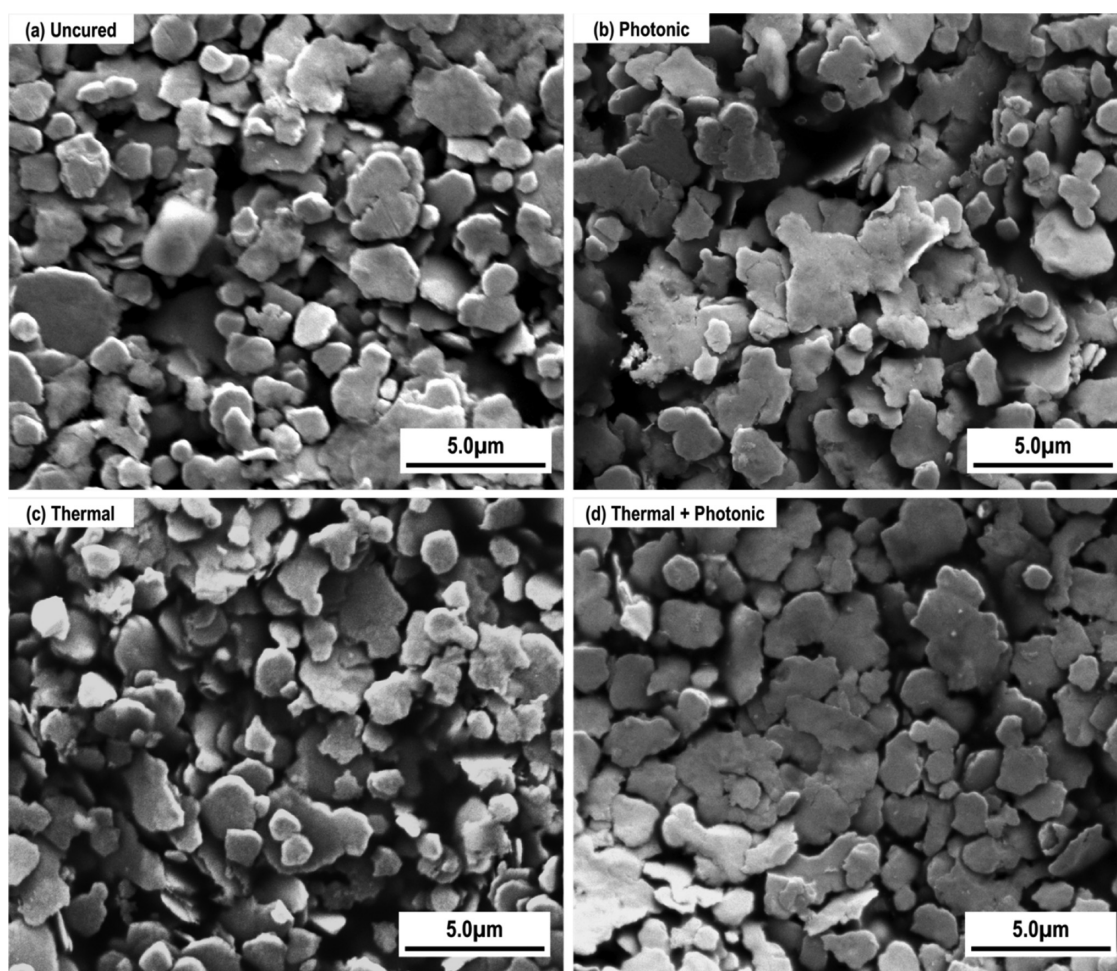


Figure 4. Typical SEM images of (a) uncured, (b) photonic, (c) thermal only, and (d) thermal and photonic cured samples. The scale bars are 5 μm .

temperature rising slightly higher. Although the precise value for the temperature rise at the front surface may differ between samples due to the complex thermal nature of the printed layers, and the fact that the assumptions outlined above may not always hold, this model shows that achieving high temperatures on the surface is possible while keeping the rear surface below the substrate melting point—a key consideration in many photonic processes.⁴⁰

Further insights into the temperature evolution were gained by the development of a simple finite-element model using the SimScale software. The same inputs and material parameters arrived at above were used as inputs to the model. The results of the temperature on the top surface of a representative silver line pattern on the third of three pulses, of 3 ms duration at 100 Hz, are shown for a number of timesteps in Figure 3c. As shown here, the maximum temperature calculated by the software matches well with that calculated analytically in Figure 3b, and the temperature field is uniform across the surface (the slight irregularities shown are artefacts of the mesh).

These calculations were compared with reality by use of radiometric temperature measurement via a thermal camera, as shown in Figure 3d. Note that the camera was not synchronized with the lamp pulse controller, and as such the long frame time of this camera (approx. 8 ms) may have led to an underestimation of the maximum sample surface temperature because the rise and fall in temperature is very rapid, on

the order of milliseconds, as shown in Figure 3b. Nevertheless, the measured temperature of approximately 275 °C is in reasonable agreement with the calculated temperature by both analytical and finite-element methods, which were 332 and 333 °C, respectively.

These results are in line with previously published experimental data on the temperature rise in similar systems, which was measured at around 200 °C for three flashes, albeit in a setup that measured the back surface temperature.²⁴ Previously reported lumped capacitance calculations by Kang et al. estimated a temperature rise of silver nanoparticles (which have very different optical properties compared with flakes) of around 500 °C,¹⁶ which is broadly consistent with our calculations outlined above considering in that study the optical energy input was almost double of that employed here.

Although the temperature rise in our system would not reach the melting point of bulk silver (962 °C), the onset of sintering in many systems is commonly observed to be several hundred degrees below the melting point. Furthermore, localized pre-melting of flakes on the surface might be initiated by localized higher temperatures, possibly owing to the plasmonic effects on the metal surfaces. Finally, due to the flattened geometry of silver flakes specifically (as compared with spheres), their edges have a high degree of curvature. Owing to the higher surface free energy of highly curved surfaces, their melting point is reduced compared to bulk.⁴¹ Therefore pre-melting is expected

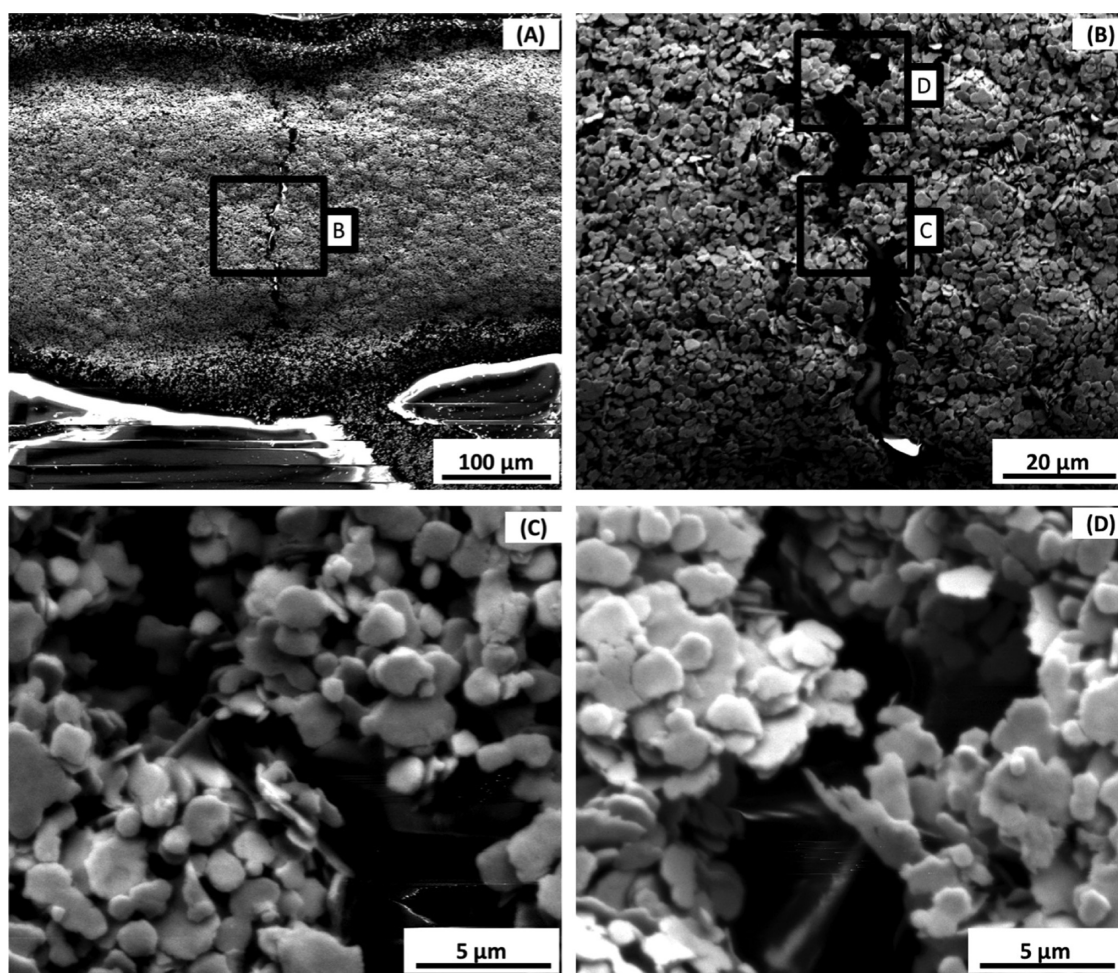


Figure 5. SEM images of F130 flake ink sample after thermal and photocuring, showing crack formation and bridging. Boxes in (A, B) show the position of the enlargements (C, D).

to initiate at the edges of flakes at temperatures significantly lower than the bulk melting temperature.

Based on these calculations and measurements, we can state that it is certainly plausible that physical changes could occur to the silver flakes. This is consistent with the hypothesis that the photonic curing can lead to partial melting and fusing of adjacent silver particles.

3.5. Characterization of Photocured Samples by SEM.

Based on the previously discussed observation of increased yield, along with the observed improvement in conductivity after photonic curing, as well as the calculated temperature rises, we hypothesized that the photonic curing has a physical effect on the samples over and above the removal of solvent, which is expected with purely thermal curing. To test this hypothesis, the samples were examined by SEM before and after photocuring, and with or without thermal curing. Typical images obtained are shown in Figure 4.

From the SEM characterization, it is clear that in no cases do the samples sinter fully, although the photonic-treated samples did show the onset of fusion between the silver flakes, as previously discussed. Given the expected pre-melting behavior discussed above, these observations support the hypothesis that fine cracks within the samples are being “healed” by the photonic treatment, leading to the increased yield observed in the electrical characterization.

To investigate this effect further, samples were stencil printed, in a manner that increased the chances of their containing fine cracks interrupting the percolation network. Note that these samples had widths ranging from 50 to 200 μm —due to this large dimensional variation, the resistivity data from these samples were not included in the averages shown in Figure 2. The samples were thermally cured and their resistance measured. The samples were then photocured and their resistance was measured again. Those samples that were not conductive after thermal curing alone (resistance $>20\text{ M}\Omega$) but became conductive after photocuring were examined by SEM. Typical SEM micrographs are shown in Figure 5.

All such samples showed the expected fine cracks, which spanned the width of the conductive line, as shown in Figure 5A and enlarged in Figure 5B. Figure 5C,D show the areas within the sample in which the crack is spanned only by a few flakes (Figure 5C), or not spanned within the examined area of the crack by only around 500 nm (Figure 5D). In such areas, it would be possible for a small expansion in mean particle size to bridge such cracks. Because this sample was not conductive after thermal curing alone (resistance $>20\text{ M}\Omega$), but became conductive after photonic curing, this provides a strong evidence that the increased yield observed in the large-scale trial can be attributed to this mechanism. Furthermore, such a “switching” behavior (in which nonconductive structures become conductive) has been previously reported²¹ in the

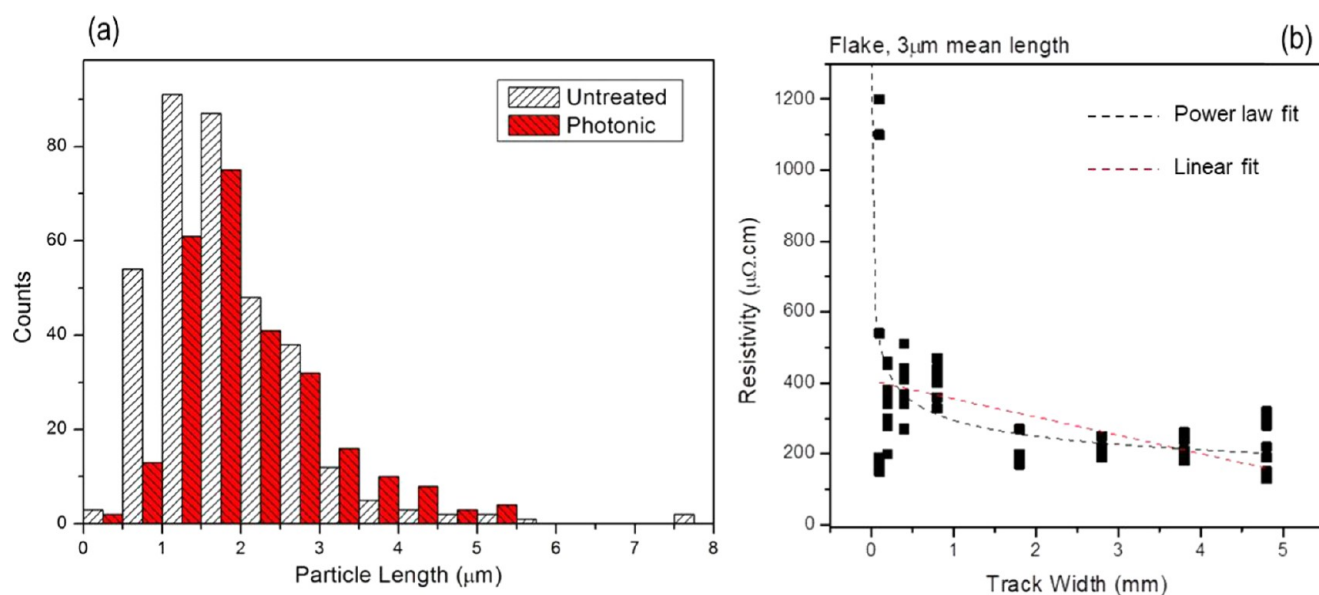


Figure 6. Histogram (a) of mean particle lengths found by automated image analysis using the software ImageJ, either photonic cured or untreated. Transfer line measurement (TLM) resistivity data (b) showing that percolation effects are important for narrow tracks containing 3 μm flakes below approximately 200 μm track width, as observed from the power-law fit to the data.

case of nanoparticle inks in response to photonic curing, but no explanation was given. Based on these observations, we conclude that crack healing may have been the mechanism responsible for the increase in yield observed.

3.6. Crack Healing and Effects of Percolation on Sample Resistivity. To further quantify the effects of particle pre-melting seen with photonic treatment, a large library of SEM images were analyzed using ImageJ software to find the particle size distribution as a function of curing regime. For this analysis, the samples were grouped into two sets; those that had not been photocured (uncured and thermal only) and those that had (photonic and thermal plus photonic). The results of this analysis are shown in Figure 6a. The mean particle size measured by this method was larger in the photonic-treated samples than in the untreated samples, increasing from 1.8 ± 0.06 to 2.10 ± 0.05 μm , respectively. A two-tailed Student's *t*-test gave a very low *p* value of <0.0003 , implying a high degree of confidence that this measured result is not a statistical fluctuation. This observation is consistent with the hypothesis that the photonic curing causes localized pre-melting at the flakes' edges. Furthermore, the size distribution of flakes in the two cases, as shown in the histogram in Figure 6, is skewed toward larger flakes for photonic treated samples and toward smaller flakes for untreated samples. This would be consistent with a mechanism causing smaller particle to fuse into larger particles, which would then be counted as one large particle with approximately double the length by the software. This increase in mean particle size, combined with the SEM analysis in Figure 5, provides strong evidence to support the crack-healing hypothesis to explain the increase in yield seen with fine line samples.

In addition to this crack-healing behavior and having established that photonic curing leads to an increase in mean particle size, we can explain the difference in resistance improvement observed between the fine line and bulk samples, by recourse to percolation theory. As the dimensions of the samples are reduced with respect to the size of the conductive particles within them, the likelihood of an individual particle

being connected to a structure that spans the entire length of the sample and therefore contributes to conduction, is reduced.⁴² This can be demonstrated by measuring resistivity as a function of track width for particles of different sizes using transfer line measurement (TLM) geometry. Such a measurement is shown in Figure 6b, which shows the resistivity of screen printed silver lines of 50 mm length and varying widths, printed from flake silver inks with a 3 μm flake size. The emergence of a power-law dependence at the narrowest track widths is visible in below track widths of approximately 200 μm . This is precisely what would be expected if percolative effects were becoming important in contributing to the overall track resistivity (i.e., the sample stops behaving as a homogeneous medium).^{42,43}

Because the line widths in the fine line photocuring experiment were 90 μm , it is likely that the fine lines are in this regime, whereas the bulk samples are not. Therefore, the fine lines' conductivity is more sensitive to small physical changes, such as healing of cracks, compared to the larger bulk samples. Therefore, photocuring can have a dramatic effect on both conductivity and yield of fine lines while having only modest effects on the physical shape and size of the particles, whereas for larger samples, the advantage of photonic curing was more minor compared with conventional thermal curing. This is an important observation because it allows the conductivity and yield of industrially interesting fine line samples to be greatly improved, by means of photonic curing, even in situations where the maximum permissible temperature is severely limited by the need to protect both binder and substrate.

3.7. Effects of Particle Size on Photonic Curing. The results above imply that there may be a correlation between particle size in the ink and performance after photocuring. To investigate this effect, aqueous silver inks containing small or large spherical particles (of 0.8 μm or 1.9 μm average diameter, respectively) were printed and photocured using the previously optimized settings, and also measured using the TLM geometry. The results are shown in Figure 7.

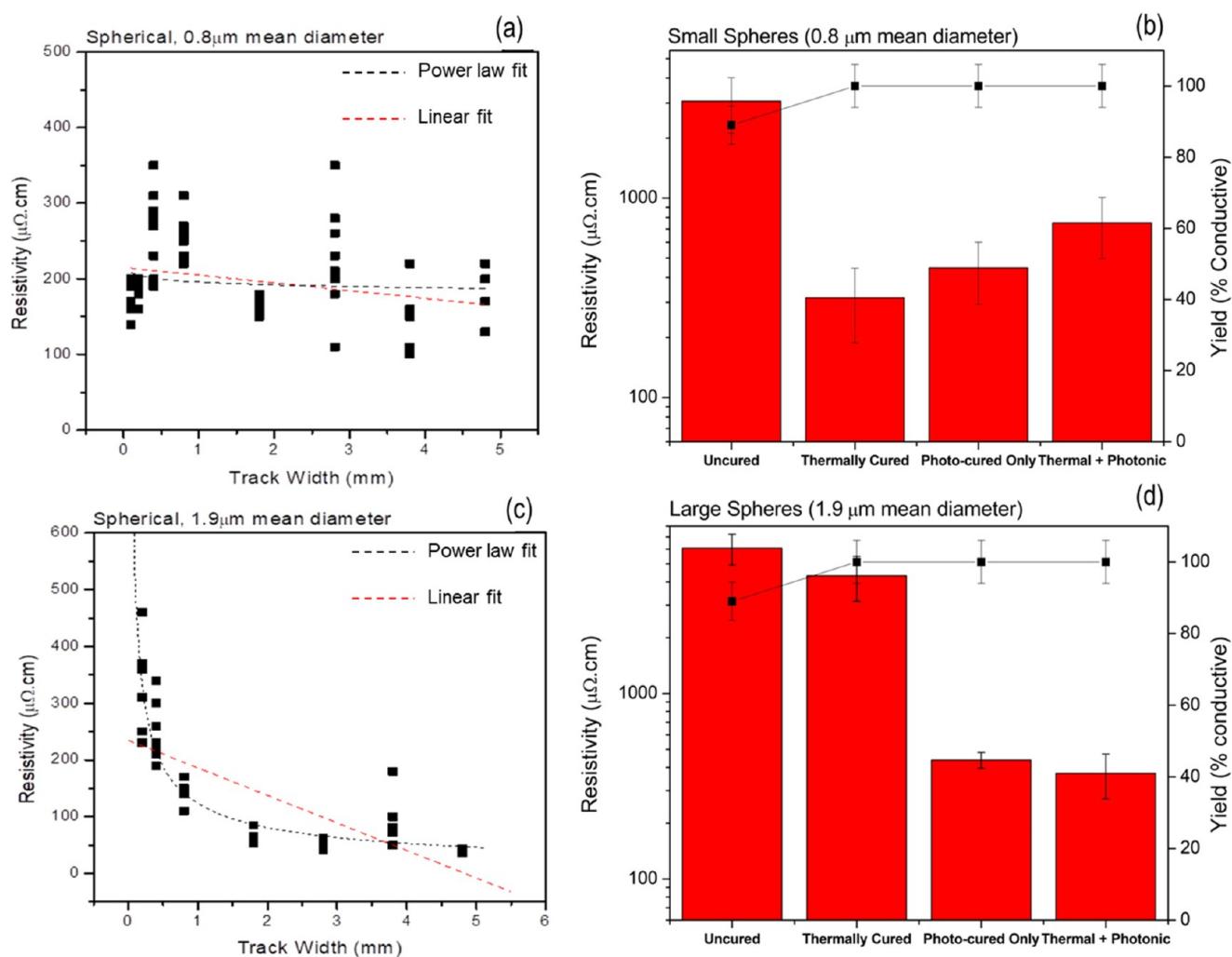


Figure 7. Resistivity of ink tracks of different widths comparing small (a) and large (c) spherical silver inks. The fits compared are linear and power-law fits of the data. Resistivity change of different particle size inks after photocuring; small spheres (b), showing no advantage of photocuring, and large spheres (d), showing an order of magnitude advantage. The yield after thermal curing was 100% in all the cases.

As shown in Figure 7a, for small particles, there is only a weak correlation between track width and resistivity. In this case, the printed ink behaves like a homogeneous material. In the case of larger particles, however, there is a clear power-law dependence of the measured resistivity on the track width, i.e., percolation is important below a track width of approximately 800 μm . This behavior was mirrored in the effects of photocuring on these two inks. As shown in Figure 7b,d, the small spheres (in which percolation was not an important consideration) showed no advantage of photonic curing over thermal curing within error, similar to the bulk flake ink samples. Larger spheres, however, showed an order of magnitude reduction in resistivity after photonic curing, as seen for the “fine line” flake ink samples. As such, percolative effects are an important consideration for explaining the response of many inks to photonic curing.

Finally, the yield of all the samples in this trial was 100% after thermal curing. This is likely due to different viscosities of the inks; however, it means we cannot comment on whether crack healing was a factor contributing to the resistivity reduction in these samples.

3.8. Effects of Photonic Curing on Flexibility of Ag Flake Inks. As previously outlined, one key advantage of flake inks that makes them interesting subjects for industrial

applications, apart from their lower cost compared with nano-sized alternatives, is their enhanced flexibility and stretchability performance. An experiment was therefore carried out to quantify any effects that photocuring may have on these properties.

Figure 8a shows the results of a bending test in which samples were bent around a 20 mm radius for up to 9000 cycles. The results, showing the average of three samples resistance/original resistance (R/R_0) are shown in Figure 8a. As shown in the figure, uncured samples showed a dramatic increase in resistance, up to 3.5 \times the original resistance. This behavior can be attributed to incomplete cross-linking of the binder in the ink when only dried at room temperature, meaning that the adhesion in the sample is poor compared to a thermally cured sample, in which the binder is more fully cross-linked. The remaining samples (thermally cured, photonic only, and thermal plus photonic) showed very similar behavior to each other; the resistance initially rose, but approached a stable value of approximately 1.2–1.3 \times the initial resistance. This demonstrates that the photonic curing has no adverse effect on the flexibility of the inks, which will be of importance for future adoption of this technology. Furthermore, because the performance of the photonic-only samples in this test was similar to that of the thermally cured samples, this implies that

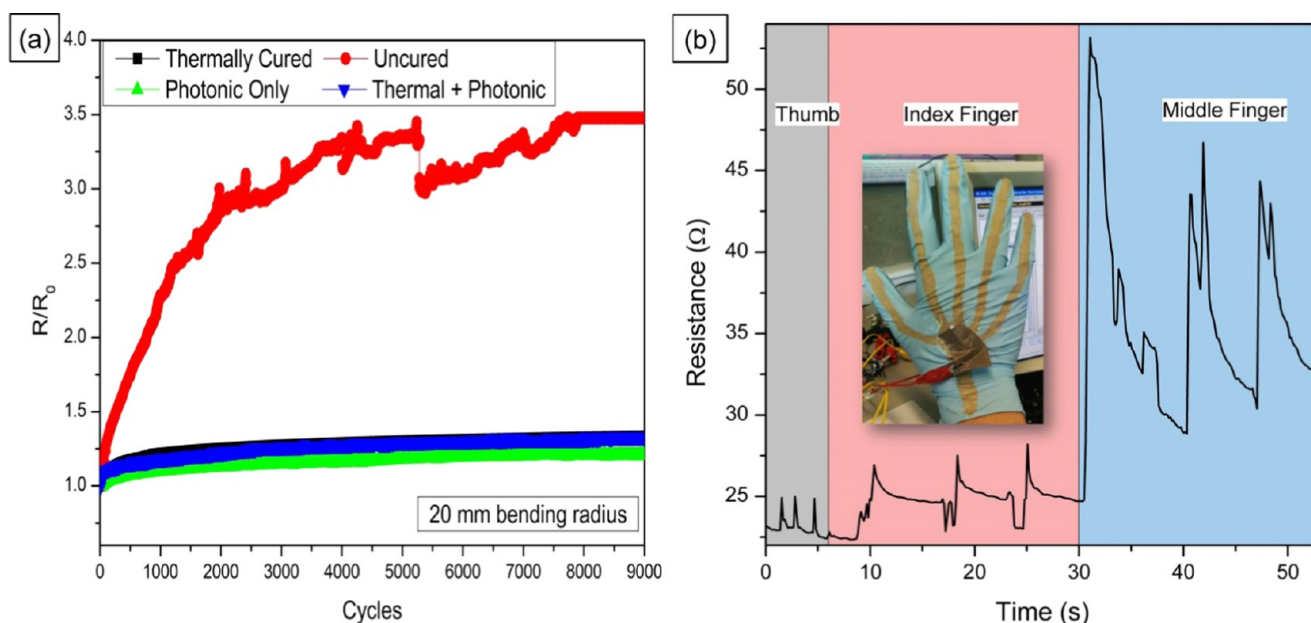


Figure 8. Flake Ag ink (a) bent around a 20 mm radius for >8000 cycles, showing that photonic curing samples retain the excellent flexibility of the thermally cured ink. Demonstration (b) of prototypical wearable sensor application (inset), with distinguishable responses to different inputs.

photonic curing is able to cross-link the binder, but in a much shorter time compared with thermal curing (9 ms vs 90 min).

Finally, as an example of a real-world application of these properties, in Figure 8b, we demonstrate the use of silver flake ink in a prototype sensor application. In this application, the printed pattern is able to distinguish clearly between different inputs. Furthermore, the ink is highly robust not only to bending (as shown in Figure 8a) but also stretching to 10% strain—as shown for thermally cured samples in Supporting Information, Figure S3. This demonstrates the potential future applications of this technology in enabling a novel form factor electronics.

4. CONCLUSIONS

Photonic curing was applied to aqueous conductive inks consisting of micron-sized silver flakes. This technique is observed to increase the conductivity over and above that which is possible by pure thermal curing. Evidence is presented that the photonic curing is able to partially pre-melt silver flakes in the ink, leading to necking between adjacent particles and healing of cracks, forming percolation pathways where none previously existed, and improving the resistivity of screen-printed fine lines from an average of $1100 \pm 230 \mu\Omega$ cm with purely thermal curing to an average of $100 \pm 12 \mu\Omega$ cm with the addition of photonic curing, whereas the most conductive patterns had a resistivity of $60 \pm 6 \mu\Omega$ cm after photonic curing. This last value corresponds to a conductivity of $(1.7 \pm 0.2) \times 10^7$ S/m.

In addition to improvements in conductivity, the yield of conductive fine lines rose from 52% with thermal curing to 80% with only photonic curing, and 100% with the optimized photonic-plus-thermal curing regime. This yield improvement is striking, and to the best of our knowledge, the first reported observation of such a yield improvement of printed conductive patterns made from water-based flake silver inks by the application of visible light photocuring. Based on the experimental and modeling work, we ascribe this effect to a

crack-healing mechanism, driven by the surface melting effects described.

As photocuring is a high-throughput, wide-area technique, we envisage that our results will be of interest to the wider printed electronics industry in terms of enabling a reduced-cost production methodology for a wide range of printed electronic components. Furthermore, although this study concentrated on flake silver inks on PET substrates, this technique is applicable to a wide range of functional materials and substrates.

■ ASSOCIATED CONTENT

Supporting Information

The Supporting Information is available free of charge on the ACS Publications website at DOI: 10.1021/acsami.8b04157.

Effect of thermal curing (Figure S1); calculated temperature profile (Figure S2); results of stretch testing (Figure S3) (PDF)

■ AUTHOR INFORMATION

Corresponding Author

*E-mail: s.silva@surrey.ac.uk.

ORCID

S. Ravi P. Silva: 0000-0002-0356-1319

Author Contributions

H.M.C. designed the experiments, collected and analyzed the data, and wrote the manuscript. Z.S. formulated the conductive inks and assisted with data collection. M.B. operated the photocuring lamp. M.S. and S.R.P.S. contributed to data analysis and editing of the manuscript. S.R.P.S., M.S., and Z.S. supervised the project. All the authors have given approval to the final version of the manuscript.

Funding

This work was supported by the U.K. Engineering and Physical Sciences Research Council (EPSRC) through the University of Surrey's Centre for Doctoral Training in MinMaT (grant no. EP/G037388). This work forms part of an EngD project, which is sponsored by DZP Technologies Ltd., Cambridge, U.K.

H.M.C. is additionally grateful for support from the Royal Commission for the Exhibition of 1851 through an Industrial Fellowship. The authors declare no competing financial interest.

Notes

The authors declare no competing financial interest.

The data supporting this article is available at <https://doi.org/10.6084/m9.figshare.6553823>.

ACKNOWLEDGMENTS

H.M.C. gratefully acknowledges Peter Reed and M.B. at Heraeus Noblelight Ltd. for their assistance with the photonic curing experiments. The authors acknowledge K. Mak at DZP Technologies Ltd. for his assistance with the TLM measurements.

REFERENCES

- (1) IDTechEx. Printed, Organic and Flexible Electronics; Forecasts Players and Opportunities 2017–2027, 2017.
- (2) Nash, C.; Spiesschaert, Y.; Amarandei, G.; Tomov, R. I.; Tonchev, D.; van Driessche, I.; Glowacki, B. A. A Comparative Study on the Conductive Properties of Coated and Printed Silver Layers on a Paper Substrate. *J. Electron. Mater.* **2014**, *44*, 497–510.
- (3) Krebs, F. C.; Jørgensen, M.; Norrman, K.; Hagemann, O.; Alstrup, J.; Nielsen, T. D.; Fyenbo, J.; Larsen, K.; Kristensen, J. A Complete Process for Production of Flexible Large Area Polymer Solar Cells Entirely Using Screen printing-First Public Demonstration. *Sol. Energy Mater. Sol. Cells* **2009**, *93*, 422–441.
- (4) Sam, F. L. M.; Razali, M. A.; Jayawardena, K. D. G. I.; Mills, C. A.; Rozanski, L. J.; Beliatas, M. J.; Silva, S. R. P. Silver Grid Transparent Conducting Electrodes for Organic Light Emitting Diodes. *Org. Electron.* **2014**, *15*, 3492–3500.
- (5) Galagan, Y.; Coenen, E. W. C.; Abbel, R.; van Lammeren, T. J.; Sabik, S.; Barink, M.; Meinders, E. R.; Andriessen, R.; Blom, P. W. M. Photonic Sintering of Inkjet Printed Current Collecting Grids for Organic Solar Cell Applications. *Org. Electron.* **2013**, *14*, 38–46.
- (6) Jung, M.; Kim, J.; Noh, J.; Lim, N.; Lim, C.; Lee, G.; Kim, J.; Kang, H.; Jung, K.; Leonard, A. D.; Tour, J. M.; Cho, G. All-Printed and Roll-to-Roll-Printable 13.56 MHz-Operated 1-Bit RF Tag on Plastic Foils. *IEEE Trans. Electron Devices* **2010**, *57*, 571–580.
- (7) Choi, Y.-M.; Kim, K.-Y.; Lee, E.; Jo, J.; Lee, T.-M. Fabrication of a Single-Layer Metal-Mesh Touchscreen Sensor Using Reverse-Offset Printing. *J. Inf. Disp.* **2014**, *16*, 37–41.
- (8) Alshammari, A. S.; Shkunov, M.; Silva, S. R. P. Inkjet Printed PEDOT: PSS/MWCNT Nano-Composites with Aligned Carbon Nanotubes and Enhanced Conductivity. *Phys. Status Solidi RRL* **2014**, *8*, 150–153.
- (9) Polino, G.; Abbel, R.; Shanmugam, S.; Bex, G. J. P.; Hendriks, R.; Brunetti, F.; Di Carlo, A.; Andriessen, R.; Galagan, Y. A Benchmark Study of Commercially Available Copper Nanoparticle Inks for Application in Organic Electronic Devices. *Org. Electron.* **2016**, *34*, 130–138.
- (10) IDTechEx. Conductive Ink Markets 2016–2026: Forecasts, Technologies, Players, 2016.
- (11) Neaikov, O. D.; Frishberg, I.; Gopienko, V.; Lotsko, D.; Mourachova, I.; Naboychenko, S.; Neikov, O. *Handbook of Non-Ferrous Metal Powders: Technologies and Applications*; Elsevier, 2009.
- (12) Yang, Y.; Seyedmohammadi, S.; Kumar, U.; Gnizak, D.; Graddy, E.; Shaikh, A. Screen Printable Silver Paste for Silicon Solar Cells with High Sheet Resistance Emitters. *Energy Procedia* **2011**, *8*, 607–613.
- (13) Frey, M.; Clement, F.; Dilfer, S.; Erath, D.; Biro, D. Front-Side Metalization by Means of Flexographic Printing. *Energy Procedia* **2011**, *8*, 581–586.
- (14) Faddoul, R.; Reverdy-Bruas, N.; Blayo, A. Formulation and Screen Printing of Water Based Conductive Flake Silver Pastes onto Green Ceramic Tapes for Electronic Applications. *Mater. Sci. Eng., B* **2012**, *177*, 1053–1066.
- (15) Nanda, K.; Sahu, S.; Behera, S. Liquid-Drop Model for the Size-Dependent Melting of Low-Dimensional Systems. *Phys. Rev. A* **2002**, *66*, No. 013208.
- (16) Kang, J. S.; Ryu, J.; Kim, H. S.; Hahn, H. T. Sintering of Inkjet-Printed Silver Nanoparticles at Room Temperature Using Intense Pulsed Light. *J. Electron. Mater.* **2011**, *40*, 2268–2277.
- (17) Lee, D. J.; Park, S. H.; Jang, S.; Kim, H. S.; Oh, J. H.; Song, Y. W. Pulsed Light Sintering Characteristics of Inkjet-Printed Nanosilver Films on a Polymer Substrate. *J. Micromech. Microeng.* **2011**, *21*, No. 125023.
- (18) Park, S.-H.; Jang, S.; Lee, D.-J.; Oh, J.; Kim, H.-S. Two-Step Flash Light Sintering Process for Crack-Free Inkjet-Printed Ag Films. *J. Micromech. Microeng.* **2013**, *23*, No. 015013.
- (19) Kang, H.; Sowade, E.; Baumann, R. R. Direct Intense Pulsed Light Sintering of Inkjet-Printed Copper Oxide Layers within Six Milliseconds. *ACS Appl. Mater. Interfaces* **2014**, *6*, 1682–1687.
- (20) West, J.; Carter, M.; Smith, S.; Sears, J. Photonic Sintering of Silver Nanoparticles: Comparison of Experiment and Theory. *Sintering: Methods Prod.* **2012**, 173–189.
- (21) Perelaer, J.; Abbel, R.; Wünscher, S.; Jani, R.; Van Lammeren, T.; Schubert, U. S. Roll-to-Roll Compatible Sintering of Inkjet Printed Features by Photonic and Microwave Exposure: From Non-Conductive Ink to 40% Bulk Silver Conductivity in Less than 15 Seconds. *Adv. Mater.* **2012**, *24*, 2620–2625.
- (22) Niittynen, J.; Sowade, E.; Kang, H.; Baumann, R. R.; Mäntysalo, M. Comparison of Laser and Intense Pulsed Light Sintering (IPL) for Inkjet-Printed Copper Nanoparticle Layers. *Sci. Rep.* **2015**, *5*, No. 8832.
- (23) Roberson, D. A.; Wicker, R. B.; MacDonald, E. Ohmic Curing of Printed Silver Conductive Traces. *J. Electron. Mater.* **2012**, *41*, 2553–2566.
- (24) Allen, M.; Alastalo, A.; Suhonen, M.; Mattila, T.; Lappaniemi, J.; Seppä, H. Contactless Electrical Sintering of Silver Nanoparticles on Flexible Substrates. *IEEE Trans. Microwave Theory Tech.* **2011**, *59*, 1419–1429.
- (25) Olkkonen, J.; Leppäniemi, J.; Mattila, T.; Eiroma, K. Sintering of Inkjet Printed Silver Tracks with Boiling Salt Water. *J. Mater. Chem. C* **2014**, *2*, 3577–3582.
- (26) Hösel, M.; Krebs, F. C. Large-Scale Roll-to-Roll Photonic Sintering of Flexo Printed Silver Nanoparticle Electrodes. *J. Mater. Chem.* **2012**, *22*, 15683–15688.
- (27) Chen, G. Y.; Stolojan, V.; Silva, S. R. P. Top-Down Heating for Low Substrate Temperature Synthesis of Carbon Nanotubes. *J. Nanosci. Nanotechnol.* **2010**, *10*, 3952–3958.
- (28) Tam, S. K.; Fung, K. Y.; Ng, K. M. Copper Pastes Using Bimodal Particles for Flexible Printed Electronics. *J. Mater. Sci.* **2016**, *51*, 1914–1922.
- (29) Park, J.; Kang, H. J.; Shin, K.-H.; Kang, H. Fast Sintering of Silver Nanoparticle and Flake Layers by Infrared Module Assistance in Large Area Roll-to-Roll Gravure Printing System. *Sci. Rep.* **2016**, *6*, No. 34470.
- (30) Cui, H.-W.; Jiu, J.-T.; Nagao, S.; Sugahara, T.; Sukanuma, K.; Uchida, H.; Schroder, K. A. Ultra-Fast Photonic Curing of Electrically Conductive Adhesives Fabricated from Vinyl Ester Resin and Silver Micro-Flakes for Printed Electronics. *RSC Adv.* **2014**, *4*, 15914–15922.
- (31) PChem Associates. Product Data Sheet—PFI-722 Conductive Flexo Silver Ink. <http://nanopchem.com/wp-content/uploads/file/DataSheets/PFI-722DataSheet.pdf> (accessed Jan 15, 2017).
- (32) Carslaw, H. S.; Jaeger, J. C. *Conduction of Heat in Solids*, 2nd ed.; The Clarendon Press: Oxford, 1959.
- (33) Çengel, Y. A.; Ghajar, A. J. *Heat and Mass Transfer: Fundamentals and Applications*, 5th ed.; McGraw Hill: New York, 2015.
- (34) Bird, R. B.; Stewart, W. E.; Lightfoot, E. N. *Transport Phenomena*, 2nd ed.; John Wiley: New York, 2007.
- (35) Jones, W.; March, N. H. *Theoretical Solid State Physics*; Wiley-Interscience: London, 1973.
- (36) Franz, R.; Wiedemann, G. Ueber Die Wärme-Leitungsfähigkeit Der Metalle. *Ann. Phys. Chem.* **1853**, *165*, 497–531.

- (37) Parker, W. J.; Jenkins, R. J.; Butler, C. P.; Abbott, G. L. Flash Method of Determining Thermal Diffusivity, Heat Capacity, and Thermal Conductivity. *J. Appl. Phys.* **1961**, *32*, 1679–1684.
- (38) Cowan, R. D. Pulse Method of Measuring Thermal Diffusivity at High Temperatures. *J. Appl. Phys.* **1963**, *34*, 926–927.
- (39) Krantz, J.; Forberich, K.; Kubis, P.; Machui, F.; Min, J.; Stubhan, T.; Brabec, C. J. Printing High Performance Reflective Electrodes for Organic Solar Cells. *Org. Electron.* **2015**, *17*, 334–339.
- (40) Beliatis, M. J.; Martin, N. A.; Leming, E. J.; Silva, S. R. P.; Henley, S. J. Laser Ablation Direct Writing of Metal Nanoparticles for Hydrogen and Humidity Sensors. *Langmuir* **2011**, *27*, 1241–1244.
- (41) Wettlaufer, J. S.; Worster, M. G. Premelting Dynamics. *Annu. Rev. Fluid Mech.* **2006**, *38*, 427–452.
- (42) Aharony, A.; Stauffer, D. *Introduction to Percolation Theory*; Taylor & Francis: London, 2003.
- (43) Grimmett, G. Near the Critical Point: Scaling Theory. In *Percolation*; Grimmett, G., Ed.; Springer: Berlin, Heidelberg, 1999; pp 232–253.